16. N. N. Smirnov, "Spinning detonation in a two-phase gas-film system," Vestn. MGU, Ser. 1, Matematika, Mekhanika, No. 2 (1980).
17. N. I. Zverev and N. N. Smirnov, "Two-phase detonation over a layer of fuel," Fiz. Goreniya Vzryva, 18, No. 1 (1982).
18. V. M. Gendugov, "Detonation of heterogeneous systems of unmixed phases," Fiz. Goreniya Vzryva, 8, No. 4 (1972).
19. S. A. Lesnyak and V. G. Slutskii, "One-dimensional diffusion model of heterogeneous (gas-film) detonation," Zh. Prikl. Mekh. Tekh. Fiz., No. 3 (1974).
20. I. N. Zverev, N. I. Zverev, and N. N. Smirnov, "Development of two-phase (gas-film) detonation," in: Gas and Wave Dynamics [in Russian], Moscow State University Press, Moscow (1981), No. 2.
21. D. I. Blokhintsev, Acoustics of a Nonuniform Moving Medium [in Russian], Nauka, Moscow (1981).
22. V. P. Glushko (ed.), Thermodynamic Properties of Individual Materials [in Russian], Izd. Akad. Nauk SSSR, Moscow (1962), Vol. 2.

ISOTHERMS AND GRÜNEISEN FUNCTIONS FOR 25 METALS

L. V. Al'tshuler, S. E. Brusnikin, and E. A. Kuz'menkov

UDC 532.593+536.715:546.3

1. Introduction. The study of the compressibility of materials at 0°K and at room temperatures is traditionally one of the main directions of research in high-pressure physics. In works devoted to this problem the sources of experimental information are "normal" isotherms recorded on static setups at T = 293°K, ultrasonic data, and especially shock-wave determinations of the Hugoniot adiabat. Based on dynamic experiments, the zero cold-compression isotherms $p_c(\rho)$ (p_c is the pressure at T = 0; ρ is the density) are found [1, 2] by separating the shock pressures into thermal and "cold" components under acceptable assumptions about the Grüneisen functions, characterizing the thermal elasticity of compressed bodies. In the widely acclaimed work [3], the isotherms of 14 metals are calculated within the framework of the Mie–Grüneisen equations of state according to the parameters of precisely measured Hugoniot adiabats and the approximate relation $\gamma\rho = \gamma_0\rho_0$ (γ is the temperature-independent Grüneisen constant). In this manner, in particular, the standard isotherms of copper molybdenum, silver and palladium, used in [4] for calibrating fluorescence ruby pressure gauges for the megabar range, were calculated. In [5-8], more complete equations of state, including the electronic components and taking into account the anharmonicity of the vibrations of the crystal lattice, were employed for the interpretation of dynamic experiments for the same purposes. The "harmonic" Grüneisen coefficients were calculated here based on different variants of the theory of small vibrations which, however, do not have any strict justifications.

Another method for constructing the curves $p_c(\rho)$ of the potential interaction and the normal isotherms $p_T(\rho)$ is based on the determination of the parameters of semiempirical potentials from the isentropic $\kappa_0 S$ or isothermal $\kappa_0 T$ bulk moduli of the initial state (T = 293°K, p = 0) and their derivatives with respect to the pressure – $\kappa_1 S$ or $\kappa_1 T$. The values of $\kappa_0 S$ and $\kappa_0 T$ were found in [9-11] by means of analytic approximations of the isotherms, recorded up to p = 4.5 GPa. Different methods of approximation yielded stable values of $\kappa_0 T$ and very different derivatives $\kappa_1 T$, which determined the extrapolation behavior of the curves. A somewhat better results using the same information was achieved in [12] in the description of isotherms by the Morse potential and by taking into account the sublimation energy, which had a stabilizing effect.

The isentropic characteristics of the initial compressibility and their isothermal analogs are revealed with high reliability by ultrasonic measurements at atmospheric and high

Minsk. Translated from Zhurnal Prikladnoi Mekhaniki i Tekhnicheskoi Fiziki, No. 1, pp. 134-146, January-February, 1987. Original article submitted October 25, 1985.

0021-8944/87/2801-0129$12.50

pressures. Ultrasonic data were employed in [13] to construct the isothermal equations of state of 11 metals, 11 ionic compounds, silicon, germanium, and sulfur. For each substance, based on the values of $\kappa_0 T$ and $\kappa_1 T$, several isotherms, having at the origin a common second-order tangent point, were found: in a form following from the Born–Mayer potential, based on the equation of the M-1 model

$$p_{T0} = \frac{3\varkappa_{0T}}{\varkappa_{1T} - 2}\left(\sigma^{\frac{2\varkappa_{1T}-1}{3}} - \sigma^{\frac{1+\varkappa_{1T}}{3}}\right), \quad \sigma = \rho/\rho_0, \tag{1.1}$$

proposed in [14], and based on the equation of state [13] with terms describing the kinetic, exchange, and correlation energy of conduction electrons. Up to $\sigma \approx 1.4$ the different analytical curves are practically identical, but for higher values of σ the isotherms of the last equation of state are significantly lower.

The previously obtained equations of isotherms have the common deficiency that they are not unique, which is attributable to the significant uncertainty in the Grüneisen functions and differential coefficients κ_1 ("static" and "ultrasonic").

Much more accurate and reliable values of the parameters of potentials and the positions of isotherms for metals with smooth adiabats were obtained in this work with the use of information obtained by combined statistical analysis of the results of ultrasonic and shock-wave measurements, first carried out in [15]. The elastic constants of uncompressed metals can be taken from the shock-wave data because of the quasihydrostatic nature of the Hugoniot states owing to the peculiar relaxation of the tangential stresses at discontinuities [15, 16] and the negligibly small effect of shock-induced melting on the form of the adiabat [17, 18].

2. Basic Relations. As the result of a statistical analysis, taking into account the latest experimental data, in this work more accurate relations for the Hugoniot adiabats in the form of dependences D(u)

$$D = a_0 + a_1 u \quad \text{and} \quad D = a_0 + a_1 u + a_2 u^2, \tag{2.1}$$

relating the wave D and mass u velocities of shock waves, are obtained for 25 metals with smooth adiabats. The first coefficients in Eqs. (2.1) determine the initial isentropic bulk moduli

$$\left(\frac{\partial p_S}{\partial \ln \rho}\right)_{p=0} = \varkappa_{0S} = \rho_0 a_0^2 \tag{2.2}$$

and the coefficients a_1, characterizing the slopes of the D(u) diagrams, determine their derivatives with respect to the pressure

$$\left(\frac{\partial \varkappa_S}{\partial p}\right)_{p=0} = \varkappa_{1S} = 4a_1 - 1. \tag{2.3}$$

For the two-parameter potential chosen the normal isentropes $p_{S0} = p_{S0}(\rho, \kappa_0 S, \kappa_1 S)$, passing through the initial states and having a point of second-order tangency with the shock adiabat at p = 0 by virtue of (2.3), are also thereby determined.

For the Debye model of a solid with a known isentrope the normal isotherm is given by

$$p_{T0} = p_{S0}(\sigma) - \gamma_\ell(\sigma)\rho\frac{3R}{A}\left[T_S D\left(\frac{\Theta_0}{T_0}\right) - T_0 D\left(\frac{\Theta(\rho)}{T_0}\right)\right] \tag{2.4}$$

and the zero isotherm for T = 0 is given by

$$p_x = p_{S0}(\sigma) - \gamma_\ell(\sigma)\rho\frac{3R}{A}\left[T_S D\left(\frac{\Theta_0}{T_0}\right)\right]. \tag{2.5}$$

Here R is the gas constant; A, atomic weight; γ_ℓ, Grüneisen coefficient of the lattice; $D(\Theta/T)$, Debye function; Θ_0, Debye temperature under normal conditions; T_0, initial temperature; $\Theta(\rho)$ and T_S, values of Θ and T under isentropic compression, determined by the relations

$$\Theta(\rho)/\Theta_0 = T_S/T_0 = \exp\left[\int_{\rho_0}^{\rho} \gamma_\ell(\rho)\, d\ln\rho\right]. \tag{2.6}$$

The exact value of the function $\gamma_\ell(\sigma)$ is not important, since for $\rho = \rho_0$ the second term in (2.4) equals zero, while for compressed states it is negligibly small compared with $pS_0(\rho)$. In what follows, in (2.4)-(2.6), the Grüneisen function of the lattice is written in the form

$$\gamma_\ell = \gamma_\infty + (\gamma_0 - \gamma_\infty)/\sigma^m,\ m = \gamma_0/(\gamma_0 - \gamma_\infty) \tag{2.7}$$

with the experimental values of $\gamma_0 = \gamma(\rho_0, T_0)$ and $\gamma_\infty = 2/3$ for all elements except alkali elements, for which $\gamma_\infty = 1/2$. The logarithmic derivative of the expression (2.7) is close to the experimental derivative [19] and the asymptotic values γ_∞ correspond to the quantum-statistical Grüneisen coefficients of the lattice under extreme degrees of compression [20, 21]. According to (2.6) and (2.7),

$$\Theta/\Theta_0 = T_S/T_0 = \sigma^{\gamma_\infty}\exp\left[\frac{\gamma_0 - \gamma_\infty}{m}\left(1 - \sigma^{-m}\right)\right]. \tag{2.8}$$

The method developed for revealing the cold-interaction potential curves makes it possible to determine independently the Grüneisen functions $\bar{\gamma}(\rho)$, characterizing the thermal elasticity of the metal in the region of the phase diagram between the shock adiabat and the zero isotherm. If $E_H(\rho)$ and $p_H(\rho)$ are the internal energy and pressure of the Hugoniot adiabat, while ES_0 and pS_0 are the same for the normal isentrope, then

$$\bar{\gamma} = \left[p_H - p_{S0} + \gamma_p\rho\frac{3R}{A}T_S D\left(\frac{\Theta_0}{T_0}\right)\right]\Big/\rho\left[\left(E_H - E_{S0} + \frac{3R}{A}T_S D\left(\frac{\Theta_0}{T_0}\right)\right]. \tag{2.9}$$

Information about the Grüneisen functions, normal isentropes, and zero isotherms is sufficient for obtaining the caloric equations of state

$$p(\rho, E) = p_{S0}(\rho) + \bar{\gamma}(\rho)\rho[E - E_{S0}(\rho)] \tag{2.10}$$

or

$$p(\rho, E) = p_x(\rho) + \bar{\gamma}(\rho)\rho[E - E_x(\rho)], \tag{2.11}$$

describing the Hugoniot adiabat and the close-lying states.

The specific form of the equations of the isentropes depends on the choice of potential, characterizing the interaction between the atoms and the electrons in the metal. The equations presented below are written in the form of functions of the parameters $\kappa_0 S$ and $\kappa_1 S$ and the variable $z = \sigma^{1/3}$ for the Born–Mayer potential

$$\begin{aligned} p_{S1} &= \frac{3\kappa_{0S}}{q-2}\left[z^2\exp\left(q\left(1 - z^{-1}\right)\right) - z^4\right], \\ q &= \frac{3}{2}\left[\kappa_{1S} - 1 + \sqrt{(\kappa_{1S} - 1)^2 - \frac{8}{3}(\kappa_{1S} - 2)}\right]; \end{aligned} \tag{2.12}$$

the Morse potential

$$p_{S2} = \frac{3\kappa_{0S}}{\alpha}z^2\left[\exp\left(2\alpha\left(1 - z^{-1}\right)\right) - \exp\left(\alpha\left(1 - z^{-1}\right)\right)\right],\ \alpha = \kappa_{1S} - 1 \tag{2.13}$$

and the Berch-Murnaghan potential

$$p_{S3} = \frac{3}{2}\kappa_{0S}\left(z^7 - z^5\right)\left[1 - \frac{3}{4}(4 - \kappa_{1S})\left(z^2 - 1\right)\right]. \tag{2.14}$$

Up to degrees of compression $\sigma \sim 1.4$ the isentropes (2.12)-(2.14) are almost identical, so that within known limits the isentropic compressibility of the metal is described by the average isentrope

$$\bar{p}_S = (1/3)(p_{S1} + p_{S2} + p_{S3}). \tag{2.15}$$

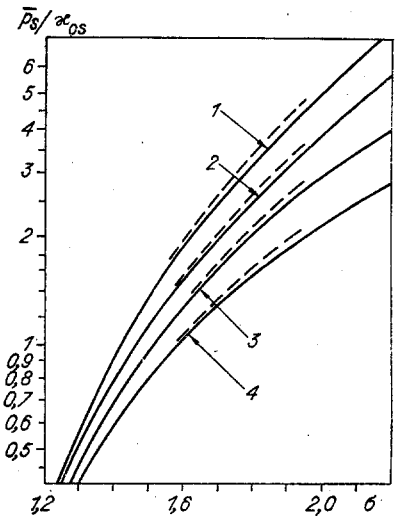

Fig. 1

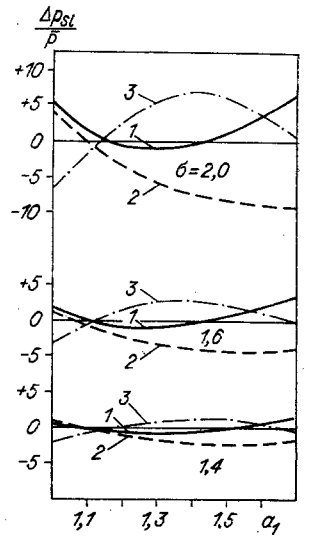

Fig. 2

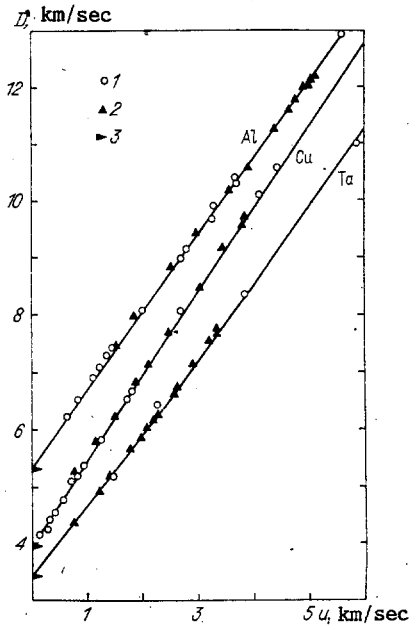

Fig. 3

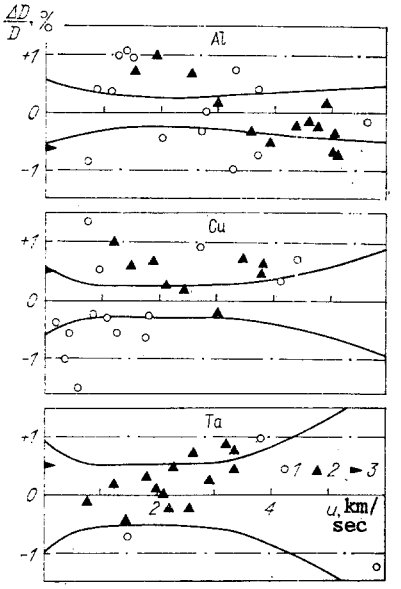

Fig. 4

In Fig. 1 the dimensionless functions $\bar{p}S/\kappa_0 S$ are shown on a semilogarithmic scale for a_1 = 1.7, 1.5, 1.3, and 1.1 (the lines 1-4, respectively). As the graph shows, the rate at which the functions grow depends largely on the parameters $\kappa_1 = 4a_1 - 1$, which must therefore be determined accurately. The relative deviations $\Delta pSi/\bar{p}S$ of the isentropes (2.12)-(2.14) from the average values (2.15) as a function of the coefficients a_1 and for different σ are shown in Fig. 2, where the lines 1-3 refer to the isentropes pS_1, pS_2, and pS_3. The disagreement between the curves increases as σ increases, but does not exceed ±2% for σ = 1.4, when the pressures in the "standard" metals Cu, Ag, Mo, and Pd already reach 100-170 GPa. The deviations for the M-1 model of Eq. (1.1) fall within the same limits (broken lines in Fig. 1). Under twofold compression the deviations from the average reach ±8%, which makes it important to choose the most realistic potential.

In this work, as in [7, 8, 22], priority is given to the Born–Mayer potential. By its qualitative agreement with the electronic theory of metals, the first term in (2.12) reflects for all elements, except alkali elements, the repulsion of the overlapping shells of the ions, while the second term reflects the Coulomb attraction of ions and free electrons. For most metals studied the Born–Mayer isentropes and isotherms are close to the curves averaged over three potentials, and for large degrees of compression they have the correct asymptotic convergence to the quantum-statistical models.

TABLE 1

Element	p_{max}, GPa	γ_0	Θ_0, K	c_0, km/sec	ρ_0, g/cm^3	a_0, km/sec	a_1	Δa_0, km/sec	$\Delta a_1 \cdot 10^2$
Li	71	0,89	448	4,792	0,534	4,769	1,065	73	1,7
Na *	34	1,31	155	2,632	0,968	2,627	1,208	26	1,3
K	90	1,34	100	2,026	0,860	1,989	1,175	25	0,9
Cu *	444	1,96	310	3,919	8,930	3,913	1,500	15	0,8
Ag *	157	2,44	221	3,129	10,490	3,146	1,651	37	3,5
Au	603	3,06	178	3,003	19,302	3,008	1,576	27	2,2
Be *	91	1,15	1031	8,028	1,851	7,993	1,128	51	2,1
Mg	177	1,60	330	4,516	1,740	4,514	1,250	40	1,4
Zn *	198	2,03	237	3,103	7,139	3,136	1,489	43	3,4
Cd *	152	2,28	221	2,467	8,639	2,474	1,642	35	3,0
Al	208	2,14	390	5,292	2,712	5,327	1,357	32	1,5
In *	155	2,43	129	2,428	7,278	2,431	1,551	34	3,0
Pb	990	2,74	87	1,972	11,346	1,976	1,568	23	2,6
V *	128	1,38	390	5,056	6,100	5,072	1,186	36	2,8
Nb *	186	1,58	260	4,444	8,586	4,440	1,192	33	2,7
Ta *	224	1,69	225	3,436	16,654	3,402	1,230	19	1,4
Mo	1041	1,61	377	5,115	10,206	5,097	1,262	27	1,3
W	542	1,76	312	4,009	19,224	4,005	1,255	21	1,6
Re	625	2,59	275	4,169	21,020	4,166	1,349	41	4,3
Co *	167	1,95	386	4,635	8,820	4,671	1,342	44	2,6
Ni *	438	1,83	345	4,542	8,875	4,540	1,507	35	2,1
Rh *	216	2,29	350	4,727	12,428	4,737	1,426	73	5,6
Pd	221	2,18	275	3,917	11,991	3,964	1,652	50	12,4
Ir	661	2,39	228	3,952	22,484	3,935	1,533	80	6,6
Pt	687	2,69	225	3,586	21,419	3,591	1,571	41	6,6

TABLE 2

Element	p_{max}, GPa	a_0, km/sec	a_1	$a_2 \cdot 10^2$, sec/km	Δa_0, km/sec	Δa_1	$\Delta a_2 \cdot 10^2$, sec/km
Na	99	2,626	1,193	+0,87	0,035	0,028	0,410
Cu	927	3,899	1,534	—0,96	0,023	0,026	0,470
Ag	460	3,137	1,744	—0,40	0,044	0,081	2,010
Be	162	7,958	1,212	—2,74	0,074	0,062	0,950
Zn	839	3,109	1,534	—1,01	0,060	0,077	1,310
Cd	863	2,456	1,734	—4,43	0,042	0,056	1,010
In	362	2,428	1,588	—1,79	0,039	0,066	1,620
Pb	990	1,976	1,568	—3,26	0,023	0,026	0,480
V	343	5,077	1,144	+2,40	0,048	0,064	1,350
Nb	409	4,446	1,117	+3,85	0,041	0,061	1,410
Ta	1136	3,418	1,193	+2,12	0,033	0,038	0,800
Co	434	4,630	1,288	+4,58	0,072	0,107	2,750
Ni	1019	4,529	1,545	—0,95	0,056	0,056	0,830
Rh	498	4,750	1,356	+4,19	0,100	0,141	3,450
Pd	221	3,964	1,652	—4,53	0,050	0,124	4,910
Pt	687	3,591	1,591	—2,81	0,041	0,066	1,640

3. Shock Adiabats and Parameters of the Potentials. The parameters of the potential and isentropic curves (2.12)-(2.14) are related by the relations (2.2) and (2.3) with the coefficients of the equations for D(u) (2.1), approximating the experimental data from ultrasonic and shock-wave measurements. The statistical analysis, based on combined approximation, of the experimental data obtained up to 1977 was carried out in [15] for all elements exhibiting metallic properties. The more accurate relations D(u) presented below for 25 metals with smooth adiabats were obtained taking into account the new measurements of the shock compressibility of aluminum, copper, and tantalum [23] and the results of investigations at the Los Alamos Laboratory, which were reexamined and supplemented in the compendium of [24] and previously partially published in [3, 25, 26]. The amount of ultrasonic information, enabling reliable extrapolation to zero pressures of the bottom sections of the shock adiabats, is also substantially enlarged owing to the data of [27], referring to single crystals.

TABLE 3

Element	$\varkappa_{1S}=4a_1-1$	$\varkappa_{1T}$[13]	$\varkappa_{1T}$[9–11]	$\varkappa_{1S}$[12]	Element	$\varkappa_{1S}=4a_1-1$	$\varkappa_{1T}$[13]	$\varkappa_{1T}$[9–11]	$\varkappa_{1S}$[12]
Cu	5,00±0,03	5,65	0,426	4,66	In	5,20±0,12	6,00	5,24	4,51
Ag	5,60±0,14	5,53	2,484	5,35	Pb	5,05±0,07	5,72	6,76	5,40
Mg	4,00±0,06	4,16	4,76	4,87	Nb	3,77±0,11	6,90	14,51	4,27
Zn	4,96±0,14	6,40	4,88	5,46	Ta	3,92±0,06	3,15	2,76	4,55
Cd	5,57±0,12	6,77	7,37	6,17	Mo	4,04±0,05	4,40	11,96	5,14
Al	4,47±0,06	4,70	3,214	4,37	Ni	5,03±0,08	6,20	20,15	4,74

As an example, illustrating the accuracy and reproducibility of the dynamic experiments, Fig. 3 shows the Hugoniot diagrams D(u) of aluminum, copper, and tantalum together with the experimental data of [6, 7, 28], obtained in the USSR (points 1) and in the USA in [23] (points 2). Figure 4 (same notation as in Fig. 3) shows for the same metals the relative confidence errors ΔD/D, calculated according to the procedure of [15], for the wave velocities as a function of their mass velocities and the deviations of specific measurements from the regression curve, constructed using the Shoven and Fischer criteria (points 3 in Figs. 3 and 4 – the most reliable volume velocities of sound c_0S under normal conditions). A significant part of the measurements of the dynamic compressibility of metals (Fig. 4) is covered by a confidence band containing with a probability of 95% the true shock adiabat, and most experimental points deviate by not more than 1% from the wave velocity of the computed Hugoniot adiabat.

The results of the statistical analysis, determining the constants in the potentials and the thermophysical characteristics, required for calculating the zero and normal isotherms, are presented in Table 1, which shows the ranges of approximations of p_{max}; the next columns shown the Grüneisen coefficients γ_0 and the Debye temperature Θ_0 from [29], the initial densities according to [24], and the most reliable velocities of sound c_0, as well as the regression coefficients a_0 and a_1 and their confidence intervals Δa_0 and $\Delta a_1 \cdot 10^2$, corresponding to a confidence probability $\alpha = 0.95$.

The shock adiabats of nine elements, after the statistical hypothesis that the linear description is applicable, was checked with the help of Fisher's criterion, were approximated with two terms $D = a_0 + a_1 u$. For the elements marked with an asterisk the initial linear intervals were separated with the use of the same criterion. The first two coefficients for the three-term relations D(u), presented in full in Table 2, are given for Pb, Pd, and Pt. Table 2 also shows the coefficients of the three-term polynomials for elements with separated linear sections.

The coefficients a_0, close in absolute magnitude to c_0, were determined with an error not exceeding 1.5%, leading to a 3% uncertainty in the bulk moduli. For the second parameter of the potentials, the confidence intervals $\Delta\varkappa_1 S = 4\Delta a_1$ for 19 elements do not exceed 0.14, for Re, Rh, and Ir they do not exceed 0.25, and for Pd the confidence interval does not exceed

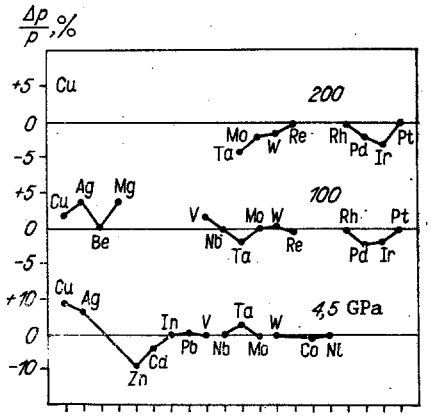

Fig. 5

TABLE 4

p, GPa	Cu	Ag	Au	Mg	Zn	Cd	Al
5	0,9659	0,9566	0,9728	0,8910	0,9376	0,9228	0,9423
10	0,9378	0,9231	0,9496	0,8219	0,8927	0,8724	0,8988
20	0,8928	0,8728	0,9116	0,7323	0,8287	0,8054	0,8349
30	0,8577	0,8354	0,8811	0,6731	0,7833	0,7600	0,7884
40	0,8289	0,8058	0,8557	0,6293	0,7482	0,7258	0,7520
60	0,7835	0,7604	0,8149	0,5667	0,6959	0,6759	0,6971
80	0,7484	0,7263	0,7829	0,5225	0,6575	0,6399	0,6564
100	0,7200	0,6991	0,7567	0,4888	0,6273	0,6119	0,6243
150	0,6664	0,6486	0,7065	0,4294	0,5723	0,5615	0,5956
200	0,6276	0,6126	0,6697	0,3893	0,5339	0,5264	0,5244
300	0,5729	0,5622	0,6171	0,3362	0,4811	0,4784	0,4679
400	0,5345	0,5272	0,5798	0,3012	0,4450	0,4457	0,4293
	In	Pb	V	Nb	Ta	Mo	W
5	0,9087	0,9099	0,9701	0,9723	0,9755	0,9819	0,9843
10	0,8516	0,8528	0,9440	0,9478	0,9537	0,9653	0,9698
20	0,7777	0,7783	0,9000	0,9062	0,9161	0,9358	0,9436
30	0,7286	0,7286	0,8638	0,8716	0,8845	0,9102	0,9205
40	0,6921	0,6915	0,8329	0,8422	0,8573	0,8876	0,8999
60	0,6394	0,6378	0,7832	0,7938	0,8122	0,8491	0,8642
80	0,6017	0,5994	0,7435	0,7552	0,7758	0,8171	0,8341
100	0,5725	0,5698	0,7108	0,7232	0,7454	0,7898	0,8082
150	0,5205	0,5167	0,6482	0,6614	0,6963	0,7355	0,7559
200	0,4846	0,4802	0,6022	0,6159	0,6422	0,6940	0,7154
300	0,4360	0,4302	0,5370	0,5508	0,5787	0,6328	0,6550
400	0,4030	0,3971	0,4913	0,5051	0,5337	0,5885	0,6108
	Re	Co	Ni	Rh	Pd	Ir	Pt
5	0,9866	0,9748	0,9742	0,9828	0,9751	0,9861	0,9825
10	0,9741	0,9527	0,9518	0,9671	0,9537	0,9732	0,9668
20	0,9514	0,9151	0,9147	0,9395	0,9184	0,9503	0,9394
30	0,9312	0,8840	0,8845	0,9157	0,8899	0,9301	0,9161
40	0,9131	0,8575	0,8590	0,8948	0,8660	0,9123	0,8958
60	0,8815	0,8140	0,8178	0,8593	0,8274	0,8816	0,8618
80	0,8546	0,7792	0,7852	0,8301	0,7970	0,8559	0,8340
100	0,8312	0,7503	0,7583	0,8052	0,7720	0,8338	0,8104
150	0,7837	0,6945	0,7067	0,7558	0,7240	0,7894	0,7640
200	0,7465	0,6531	0,6686	0,7181	0,6887	0,7550	0,7289
300	0,6905	0,5935	0,6140	0,6625	0,6379	0,7036	0,6772
400	0,6491	0,5513	0,5752	0,6222	0,6018	0,6659	0,6397

TABLE 5

p, GPa	Li	K	Na	Be	p, GPa	Li	K	Na	Be
1	0,9272	0,8089	0,8820	0,9915	9	0,6691	0,4784	0,5922	0,9336
2	0,8723	0,7147	0,8093	0,9834	10	0,6516	0,4622	0,5756	0,9273
3	0,8482	0,6528	0,7570	0,9755	20	0,5328	0,3607	0,4681	0,8730
4	0,7918	0,6073	0,7163	0,9680	30	0,4637	0,3072	0,4084	0,8299
5	0,7607	0,5716	0,6832	0,9606	40	0,4164	0,2722	0,3683	0,7942
7	0,7097	0,5179	0,6316	0,9467	50	0,3811	0,2469	0,3386	0,7638

0.50. As can be seen from Table 3, the values found by other methods lead to much higher uncertainties. The quantities $\kappa_1 S = 4a_1 - 1$ are compared here for 12 elements with ultrasonic determinations of $\kappa_1 S$, employed in [13], and with the data based on the approximation of the isothermal compression curves both in the original works [9-11] and in the interpretation of [12].

The accurate determination of the values of $\kappa_1 S$, determining the extrapolation properties of the potentials, is one of the main results of the statistical analysis carried out in [15] and in this work.

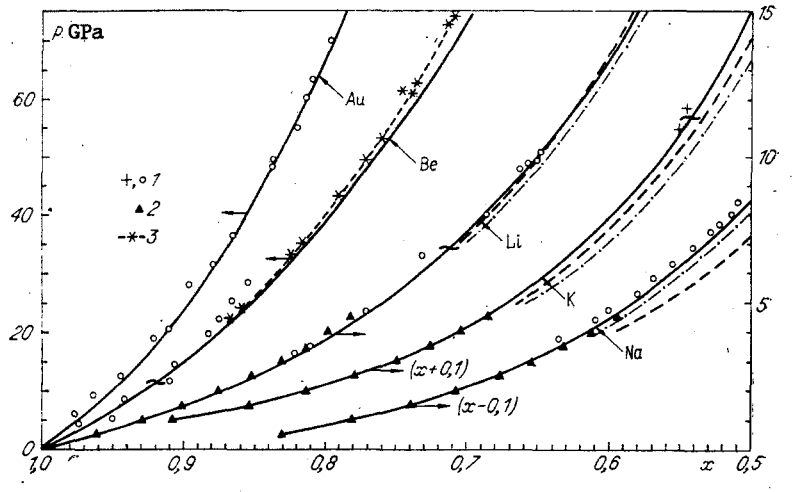

Fig. 6

On the whole, Table 1 contains all the information required to construct with the required accuracy the normal isentropes appearing in the caloric equations of state, the normal and zero isotherms, and the Grüneisen functions.

4. Normal Isotherms. For a chosen potential the normal isotherms are determined by the characteristics of the initial state ρ_0, γ_0, Θ_0 and the regression coefficients a_0 and a_1 of the adiabats in Table 1. For the Born–Mayer potential the relative volumes of the normal isotherms, calculated according to these parameters and the equations (2.2)-(2.4), (2.7), (2.8), and (2.12) in the megabar range, are presented for 21 elements in Table 4 and for Be and alkali elements in Table 5.

The tabulated isotherms are compared in Fig. 5 with the static measurements of the compressibility [9, 10] up to 4.5 GPa and the isotherms calculated in [3] based on the dynamic adiabats and the relations $\gamma\rho = \gamma_0\rho_0$ up to 200 GPa. The differences, in percent, in the pressures of the previous and new isotherms are shown here for three pressures: 4.5, 100, and 200 GPa. For the lowest pressure the experimental isotherms of eight elements agree, according to [9, 10], with the calculations; for tantalum and cadmium they differ in the pressure by 3.5%, and for copper, silver, and zinc they differ by 7-9%. The static measurements for these elements differ to such an extent from the ultrasonic data that the static measurements are probably not accurate. The tabulated curves deviate from the isotherms calculated in [3] at 100 and 200 GPa by not more than 3%.

The comparison in Fig. 6, constructed in the p–x plane ($x = \rho_0/\rho$), of the compressibility predicted in this work with the latest experimental results (points 1) for the isotherms of Au up to 70 [30], Be up to 30 [31], and Li [32], K [33], and Na [34] up to 10 GPa is of special interest. Experiments with gold and potassium were performed on diamond anvils [35], where the pressures were determined with ruby fluorescence gages. In experiments with lithium and sodium x-ray diffraction pictures of the structures of LiF and NaF, whose isotherms were determined in [36] and used as pressure strain gages, were obtained simultaneously in the compression process.

For all elements the experimental points [30-34] and previous data [11] up to 4.5 GPa (points 2) for alkali metals fall with good accuracy on the isotherms computed in this work. The three top static measurements on beryllium are exceptions. They lie above the Hugoniot adiabat of beryllium [24] (the symbol 3) and therefore refer to nonequilibrium states of anisotropic compression. The calculations also agreed with experiments for the new crystalline modifications of beryllium, lithium, and potassium, forming under pressures marked by the wavy lines, indicating the small effect of phase transitions occurring at high pressures on the elastic characteristics of the metals.

The zero and normal isotherms of alkali metals are a traditional object of study in many theoretical and experimental studies [37-41]. The isotherms shown by the dot–dashed lines from [39], obtained by reduction of the experimental Hugoniot adiabats [37, 38], substantially overestimate the compressibility of alkali metals. Potassium and lithium are realistically described by the isothermal equation [13] (broken lines), but the compressibility of sodium is overestimated even more strongly than in [39]. The adequacy of the new

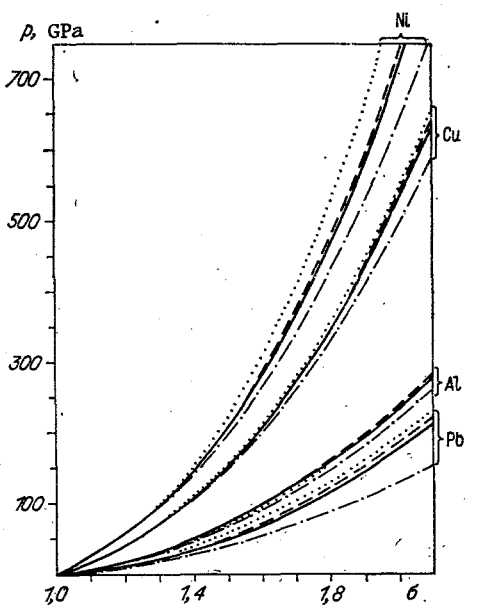

Fig. 7

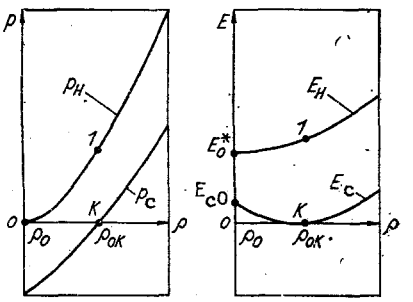

Fig. 8

TABLE 6

Element	ρ_{0K}	$\varkappa_{0K}$	q	E_0^*	Element	ρ_{0K}	$\varkappa_{0K}$	q	E_0^*
Li	0,54	12,70	5,373	0,5745	V	6,13	158,61	6,661	0,0845
Na	1,02	7,56	6,904	0,2661	Nb	8,61	170,65	6,727	0,0572
K	0,91	3,87	6,540	0,1696	Ta	16,67	193,95	7,148	0,0291
Cu	9,02	140,78	10,242	0,0759	Mo	10,24	267,08	7,507	0,0457
Ag	10,62	107,98	12,012	0,0512	W	19,31	310,77	7,428	0,0261
Au	19,49	178,59	11,131	0,0298	Re	21,12	367,68	8,495	0,0273
Be	1,86	119,16	6,032	0,1919	Co	8,88	195,52	8,416	0,0737
Mg	1,77	36,67	7,372	0,1794	Ni	8,95	187,52	10,324	0,0863
Zn	7,26	73,77	10,114	0,0833	Rh	12,49	281,98	9,383	0,0444
Cd	8,80	56,11	11,906	0,0496	Pd	12,04	192,23	12,024	0,0480
Al	2,73	78,56	8,588	0,1610	Ir	22,58	352,25	10,628	0,0282
In	7,44	45,75	10,838	0,0550	Pt	21,54	280,41	11,072	0,0280
Pb	11,59	47,11	10,394	0,0324					

curves for Na and K is also confirmed by theoretical calculations of the compressibility [41], performed up to pressures of 30 GPa by the local-pseudopotential method.

5. Zero Isotherms. The method, developed in this work, for determining the compressibility makes it possible to evaluate critically the previously obtained zero isotherms under multimegabar pressures. In [5-8] the zero isotherms of aluminum, copper, nickel, and lead were determined for a wide range of densities from dynamic data. Figure 7 shows (solid lines) in the $p_c(\sigma)$ plane the cold-compression curves of these metals, calculated using Eq. (2.5) in the Born–Mayer variant. The broken curves of the Cormer–Urlin–Funtikov equations of state [5], which take into account realistically the electronic components and anharmonicity of the vibrations of the crystalline lattice, are practically identical to them. The same situation occurs for aluminum, lead, and copper for $p_c(\rho)$ (dotted lines) based on close equations of state in [6, 7]. The appreciable overestimation of the compression pressures for nickel in [7] is attributable to the incorrect choice of the Grüneisen coefficient of the electrons ($\gamma_{el} = 0.5$), too low for transition metals. The zero isotherms (dot–dashed lines) suffer from the opposite problem: the "cold" pressures are strongly underestimated [8].

The equations of the zero isotherms in the form (2.5) contain temperature-dependent Debye terms, compensating the thermal components of the isentropic compression of the normal isentropes. To construct thermodynamically complete equations of state it is desirable to represent the cold-compression curves, including the pressure of the zero-point vibrations,

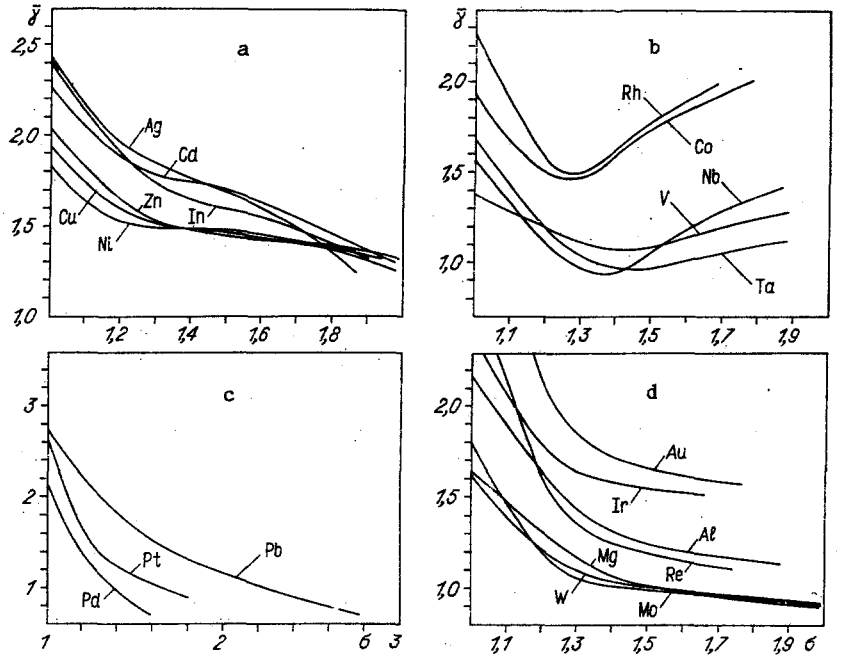

Fig. 9

by analytical potential functions of the density only in the form (2.12)-(2.14). In the equations normalized to the density $\rho_0 K$ (Fig. 8) at T = 0 and p = 0, the parameters κ_1 are assumed to be constant, while the moduli $\kappa_0 K = \rho_0 K a_0^2 K$, are expressed in terms of $\rho_0 K$ and the velocity of sound $a_0 K$ at the new zero point K in Fig. 8, where p = 0 and, by definition, E = 0.

The value of $\rho_0 K$ is found by exploiting the circumstance that in the Hugoniot state 1 the energy and pressure are of a thermal nature, and, therefore, $pH_1 = \rho_0 K \gamma_0 K E H_1$. Since

$$p_{H1} = \rho_0 u_1 (a_0 + a_1 u_1), \quad \gamma_{0K} \simeq \gamma_0 \frac{\rho_0}{\rho_{0K}}, \quad E_{H1} = E_0^* + \frac{u_1^2}{2}, \tag{5.1}$$

we have, with the required accuracy,

$$u_1 = \frac{\gamma_0 E_0^*}{a_0}, \quad \rho_{0K} = \rho_0 \left(1 + \frac{u_1}{a_0}\right). \tag{5.2}$$

Equation (5.2) contains the difference of the internal energies in the states ρ_0 and $\rho_0 K$

$$E_0^* = \frac{3R}{A} T_0 D\left(\frac{\Theta_0}{T_0}\right) + \int_{\rho_0}^{\rho_{0K}} \frac{p_c}{\rho^2} d\rho \tag{5.3}$$

where the second term is a small fraction of E_0^* (of the order of 1%). Equations (5.1)-(5.3) determine $\rho_0 K$, u_1, and also the velocity of the shock wave $D_1 = a_0 + a_1 u_1$, while the values of u_1 and D_1 in their turn determine the derivative of the dynamic adiabat

$$\left(\frac{dp}{d\rho}\right)_H = \frac{(D_1 + u_1 D_u')}{(D_1 - u_1 D_u')}(D_1 - u_1)^2 \quad (D_u' = a_1)$$

near the pole of the adiabat corresponding to the isentropic derivative cS_1^2. Finally, based on the Mie–Grüneisen equations and the relations $\gamma\rho \simeq \gamma_0 \rho_0$ for $\rho_0 K$

$$a_{0K}^2 = c_{S1}^2 - \frac{\gamma_{0K} p_{H1}}{\rho_{0K}} = c_{S1}^2 - \left(\frac{\rho_0}{\rho_{0K}}\right)^2 \gamma_0 u_1 D_1.$$

Comparison of $a_0 K$ with the experimental ultrasonic data of [27] and $\rho_0 K$ with the results of calculations of this quantity based on the coefficients of linear expansion presented for a number of metals in [42] showed good agreement with experiment.

TABLE 7

γ \ σ	1,00	1,20	1,30	1,40	1,60	1,80	2,00	2,20
Cu	1,96	1,59	1,51	1,49	1,44	1,32	1,21	1,13
Ag	2,43	1,94	1,84	1,77	1,56	1,35	—	—
Au	3,06	2,13	1,84	1,73	1,63	1,57	—	—
Mg	1,63	1,29	1,26	1,06	0,96	0,94	0,89	0,84
Zn	2,03	1,65	1,53	1,50	1,43	1,37	—	—
Cd	2,28	1,88	1,78	1,76	1,64	1,41	1,20	—
Al	2,14	1,62	1,44	1,30	1,20	1,16	—	—
In	2,42	1,91	1,74	1,65	1,52	1,41	—	—
Pb	2,74	2,29	2,02	1,81	1,52	1,33	1,15	1,03
Mo	1,61	1,16	1,06	1,01	0,98	0,95	0,92	0,88
W	1,76	1,24	1,10	1,04	0,95	0,92	0,90	—
Re	2,29	1,59	1,36	1,62	1,15	1,10	—	—
Ni	1,83	1,54	1,49	1,48	1,46	1,37	—	—
Pd	2,18	1,40	1,12	0,95	0,68	—	—	—
Ir	2,39	1,73	1,62	1,58	1,53	—	—	—
Pt	2,69	1,64	1,35	1,21	1,04	0,90	—	—

Table 6 presents the parameters of the zero isotherms, the values $\kappa_0 K = \rho_0 K a_0^2 K$, and the parameters q (2.12), calculated from the data in Table 1.

The assumptions that κ_1 and q are constant at ρ_0 and $\rho_0 K$ is not completely accurate, since in the general case the derivatives of the bulk modulus with respect to the pressure are functions of the density. Because ρ_0 and $\rho_0 K$ are close, however, the difference between the cold-compression curves constructed from Table 5 and the results obtained from the formula (2.5) does not exceed 2% at the maximum degrees of compression.

6. Grüneisen Function. The method developed for determining the potentials permits seeking independently the Grüneisen functions (2.9), characterizing the thermal elasticity of metals for states lying between the shock adiabat and the zero isotherm. The thermal components of the shock pressures and energies, determining $\bar{\gamma}(\sigma)$ increase as the degree of compression increases and as the second coefficient in the dependences D(u) (2.1) increases. As the analysis showed, significant information about the functions $\bar{\gamma}(\sigma)$ can be obtained for metals with $a_1 \gtrsim 1.2$. Based on this criterion, beryllium with $a_1 = 1.132$ and close Hugoniot adiabats and isotherms (see Fig. 6) and the alkali metals are not studied.

The functions $\bar{\gamma}(\sigma)$ for elements with linear dependences D(u) which hold throughout the experimental ranges are shown in Fig. 9d. The compression of metals in this group leads first to rapid and then to slow decrease in the thermal elasticity, which agrees qualitatively with the dynamic theory of crystal lattices. A repeated sharp drop in the curves $\bar{\gamma}(\sigma)$ is observed for $\sigma \gtrsim 1.6$ for the elements, if the upper branches of their adiabats are described by the dependences D(u) with negative coefficients a_2 (Fig. 9a).

The interrelated decrease in the slopes and Grüneisen functions is attributable to the progressive increase as a function of the degree of compression in the relative fractions of the thermal components and the simultaneous reduction owing to the anharmonicity of the lattice vibrations and thermal excitation of electrons. The same tendency determines the configuration of the curves $\bar{\gamma}(\sigma)$ (Fig. 9c) for palladium, lead, and platinum.

Transition metals with increasing derivatives D_u' ($a_2 > 0$) have nonmonotonic (anomalous) functions $\bar{\gamma}(\sigma)$ (Fig. 9b). The elevated resistance of metals to shock compression is attributable here to their high electronic heat capacities and electronic Grüneisen coefficients [29].

Selected values of the coefficients in the ranges of dynamic experiments are presented for 16 elements with monotonic dependences in Table 7.

As a whole, this work shows that the method developed has extensive possibilities and permits obtaining, without additional nonrigorous assumptions, reliable and accurate information about the isothermal compressibility and Grüneisen functions of materials with smooth shock adiabats from shock-wave and ultrasonic data.

We thank T. M. Platova and E. A. Shchegolev for discussions, which stimulated this work, and S. V. Kasatochkin and V. V. Kechin for useful discussions of a number of aspects of this work.

LITERATURE CITED

1. Dynamic Investigations of Solids at High Pressures [Russian translation], Mir, Moscow (1965).
2. L. V. Al'tshuler, "Application of shock waves in high-pressure physics," Usp. Fiz. Nauk, No. 2 (1965).
3. R. McQueen, S. P. Marsh, et al., in: High-Velocity Impact Phenomena, R. Kinslow (ed.), Academic Press, New York (1970).
4. H. K. Mao, P. M. Bell, et al., "Specific volume measurements of Cu, Pd, and Ag and calibration of the ruby fluorescence pressure gauge from 0.06 to 1 Mbar," J. Appl. Phys., 49, No. 6 (1978).
5. S. B. Kormer, A. I. Funtikov, et al., "Dynamic compression of porous metals and the equation of state with variable heat capacity at high temperatures," Zh. Éksp. Teor. Fiz., 42, No. 3 (1962).
6. L. V. Al'tshuler, S. B. Kormer, et al., "Equations of state of aluminum, copper, and lead at high pressures," Zh. Éksp. Teor. Fiz., 38, No. 3 (1960).
7. L. V. Al'tshuler, A. A. Bakanova, and R. F. Trunin, "Shock adiabats and zero isotherms of seven metals at high pressures," Zh. Éksp. Teor. Fiz., 42, No. 1 (1962).
8. V. N. Zharkov and V. A. Kalinin, Equation of State of Solids at High Pressures and Temperatures [in Russian], Nauka, Moscow (1968).
9. S. N. Vaidya and G. C. Kennedy, "Compressibility of 18 metals to 45 kbar," J. Phys. Chem. Solids, 31, No. 10 (1970).
10. S. N. Vaidya and G. C. Kennedy, "Compressibility of 22 elemental solids to 45 kbar," J. Phys. Chem. Solids, 33, No. 7 (1972).
11. S. N. Vaidya and G. C. Kennedy, "The compression of the alkali metals to 45 kbar," J. Phys. Chem. Solids, 32, No. 11 (1971).
12. E. A. Shchegolev, "Semiempirical equations of state and shock adiabats of solids," Author's Abstract of Candidate's Dissertation, Tomsk University (1981).
13. U. Walzer, "A new equation of state for high compression," Phys. Earth Planetary Interiors, 30, No. 1 (1982).
14. W. Ullman and V. L. Pankov, "A new structure of the equation of state and its application in high pressure and geophysics," Veroff. Zentralinst. Physik d. Erde, No. 41 (1976).
15. L. V. Al'tshuler, A. A. Bakanova, et al., "Shock adiabats of metals. New data, statistical analysis, and general characteristics," Zh. Prikl. Mekh. Tekh. Fiz., No. 2 (1981).
16. W. C. Moss, "Effect of material strength on the relationship between the principal Hugoniot and quasi-isentrope of beryllium and 6061-T6 aluminum below 35 GPa," J. Appl. Phys., 57, No. 5 (1985).
17. V. D. Urlin, "Melting at ultrahigh pressures, obtained in a shock wave," Zh. Éksp. Teor. Fiz., 49, No. 2 (1965).
18. Y. Horie, "Melting and the Hugoniot equation," J. Phys. Chem. Solids, 28, 1569 (1967).
19. R. Boehler, "Experimental results on the pressure dependence of Grüneisen parameter: A review," J. Geophys. Res., 85, No. B12 (1980).
20. J. J. Gilvarry, "Grüneisen's law and fusion curve at high pressure," Phys. Rev., 102, No. 2 (1955).
21. V. P. Kopyshev, "Grüneisen constant in the Fermi–Thomas approximation," Dokl. Akad. Nauk SSSR, 161, No. 5 (1965).
22. B. I. Davydov, "Equations of state of solids," Izv. Akad. Nauk SSSR, Ser. Geofiz., No. 12 (1956).
23. A. C. Mitchell and W. J. Nellis, "Compression of aluminum, copper, and tantalum," J. Appl. Phys., 52, No. 5 (1981).
24. LASL Shock Hugoniot Data, Berkeley (1979).
25. M. H. Rice, R. G. McQueen, and J. M. Walsh, "Equation of state for eleven metals," in: Solid State Physics (1958), Vol. 6.
26. R. G. McQueen and S. P. March, "Equation of state for nineteen metallic elements," J. Appl. Phys., 31, No. 7 (1960).
27. G. Simmons and H. Wang, Single Crystal Elastic Constants and Calculated Aggregate Properties: A Handbook, MIT Press (1971).
28. K. K. Krupnikov, A. A. Bakanova, et al., "Study of the shock compressibility of titanium, molybdenum, tantalum, and iron," Dokl. Akad. Nauk SSSR, 148, No. 6 (1963).
29. K. A. Gshneider, "Physical properties and interrelationships of metallic and semimetallic elements," in: Solid State Physics (1964), Vol. 16.

30. D. L. Heinz and R. Jenloz, "The equation of state of the gold calibration standard," J. Appl. Phys., 55, No. 4 (1984).
31. L. C. Ming and M. M. Manghnani, "Isothermal compression and phase transition in beryllium to 28.3 GPa," J. Phys. F: Met. Phys., 14 (1984).
32. B. Olinger, "Lithium compression and high-pressure structure," Science, 219, No. 4588 (1983).
33. H. Olijnyk and W. B. Holzapfel, "Phase transition in K and Pb under pressure," Phys. Lett. A, 99, No. 8 (1983).
34. J. N. Fritz and B. Olinger, "Equation of state of sodium," J. Chem. Phys., 80, No. 6 (1984).
35. S. Blok and G. P'ermarini, "Diamond anvils open up new possibilities in high-pressure physics," Usp. Fiz. Nauk, 127, No. 4 (1979).
36. W. J. Carter, "Hugoniot equation of state of some alkali halides," High Temp.-High Press., 5 (1973).
37. A. A. Bakanova and I. P. Dudoladov, "Compression of alkali metals by strong shock waves," Fiz. Tverd. Tela, 7, No. 6 (1965).
38. M. M. Rice, "Pressure-volume relations for the alkali metals from shock-wave measurements," J. Phys. Chem. Solids, 26, No. 3 (1965).
39. R. Grover and G. C. Kennedy, "On the compressibility of the alkali metals," J. Phys. Chem. Solids, 30 (1969).
40. V. G. Vaks, S. P. Kravchuk, and A. V. Trofimov, "Equation of state and volume dependence of the thermodynamic properties of alkali metals," Fiz. Tverd. Tela, 19, No. 5 (1977).
41. D. A. Young and M. Ross, "Theoretical high-pressure equations of state and phase diagrams of the alkali metals," Phys. Rev. B, 29, No. 2 (1984).
42. S. I. Novikova, Thermal Expansion of Solids [in Russian], Nauka, Moscow (1974).

PHENOMENOLOGICAL DESCRIPTION OF THE DISLOCATION MECHANISM OF FORMATION OF NUCLEATED DEFECTS IN PLASTIC DEFORMATION

A. A. Movchan

UDC 539.4

The phenomenological approach to the problem of describing the process of fracture consists of introducing damage parameters and kinetic equations [1] or functionals [2] which give their change during loading. This approach was first used in [3, 4] to study damage accumulation during plastic deformation. The system of phenomenological description may not correspond to the micromechanism of the processes taking place, but the presence of a physical interpretation makes such a description more reliable. Here we attempt to construct a phenomenological model of damage accumulation with the well-known dislocation mechanism of growth of nucleated defects.

In accordance with [5], dislocations moving during deformation encounter such obstacles as grain boundaries, subgrains, cells, particles of a secondary phase, etc., and accumulate at these sites, forming small regions with a high density of one type of dislocation. When the number of dislocations in the pileup exceeds a certain critical value, they combine: the pileup disappears and a nucleated defect takes its place. Thus, the process by which dislocations participate in the formation of defects can be tentatively subdivided into two stages: accumulation of dislocations at barriers; combination (disappearance) of the dislocations with the formation of a nucleated defect.

For the mechanism of defect formation proposed in [6] – connected with slip lines overcoming grain boundaries – the first stage is the accumulation of dislocations on corresponding boundaries characterized by a difference in the Burgers vector. The second stage is the formation of the defect (with the disappearance of the Burgers vector difference). For

Moscow. Translated from Zhurnal Prikladnoi Mekhaniki i Tekhnicheskoi Fiziki, No. 1, pp. 147-155, January-February, 1987. Original article submitted September 13, 1985.

